Publishing House
AKAPIT

COMPUTER METHODS IN MATERIALS SCIENCE
Informatyka w Technologii Materiałów

Vol. 16, 2016, No. 3

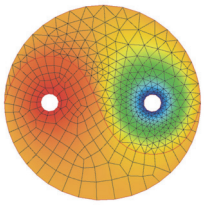

A PARALLELIZED MODEL FOR COUPLED PHASE FIELD AND CRYSTAL PLASTICITY SIMULATION

MINGXUAN LIN*, ULRICH PRAHL

Steel Institute, RWTH Aachen University, Germany
**Corresponding author: mingxuan.lin@iehk.rwth-aachen.de*

Abstract

The predictive simulation of materials with strong interaction between microstructural evolution and mechanical deformation requires the coupling of two or more multi-physics models. The coupling between phase-field method and various mechanical models have drawn growing interests. Here, we propose a coupled multi-phase-field and crystal plasticity model that respects the anisotropic mechanical behavior of crystalline materials. The difference of computational complexity and solver requirements between these models presents a challenging problem for coupling and parallelization. The proposed method enables parallel computation of both models using different numerical solvers with different time discretization. Finally two demonstrative examples are given with an application to the austenite-ferrite transformation in iron-based alloys.

Key words: Phase field, crystal plasticity, OpenMP, parallelization

1. INTRODUCTION

Continuum mechanics models and thermo-chemistry models have greatly accelerate the design and optimization of inhomogeneous materials such as composites and multiphase alloys. With the development of advanced manufacture techniques and the growing demands on extreme service conditions, materials go through complex thermo-mechanical processes during their lifecycles, in which microstructure evolution often accompanies the elasto-plastic deformation. Two well-known examples are dynamic recrystallization during forging and transformation induced plasticity in steels. Therefore, there exists increasing interest in coupling thermo-chemistry models with continuum mechanics models to simulate the mutual interaction between the chemical and mechanical processes.

The multi-phase-field method (MPF), extended from the pioneer works of Cahn and Hilliard (1958), has found wide application in the simulation of microstructure evolution with various mechanisms, including dendritic solidification, solid-solid phase transformation, recrystallization and grain growth (Steinbach & Pezzolla,1999; Steinbach & Apel, 2006; Steinbach, 2009). Recent attempts have been made to simulate incoherent martensitic and bainitic transformations in steels by adding additional terms for strain energy (Arif & Qin, 2013, 2014; Qin & Bhadeshia, 2009) or coupling with a dislocation density field (Kundin et al., 2011; Kundin et al., 2015). In the MPF model, different phases and grains are represented by individual order-parameters, with a value range from 0 to 1. The evolution equations of MPF model can be solved by finite difference (FD) or finite element (FE) method on a regular grid. However, the main-stream commercial and open-source MPF software packages adopt the finite difference scheme, primarily for better memory efficiency of storing the order parameters. Both packages made use of shared-memory CPU parallelization techniques (OpenMP). While

 ISSN 1641-8581

MPF is a strong tool to model the chemical processes, the crystal plasticity (CP) model has demonstrated strong predictivity of both local and averaged mechanical behavior of single- and multi-phase alloys ((Roters et al., 2011; Roters et al., 2010; Ma et al., 2006). It consists of a set of kinematic and constitutive equations taking into account the underlying physical phenomena, such as dislocation slip and deformation twinning. These equations are solved at every material point using the Newton-Raphson method. The most common solver for the mechanical boundary value problems with CP model is the FE method. In the past decade, a spectral method based on the fast Fourier transformation (FFT) has emerged as an alternative to FEM for problems with periodic boundary conditions. It is consider one or two order of magnitude faster than FEM (Diehl, 2010; Prakash & Lebensohn, 2009). The spectral method can be easily parallelized via OpenMP and MPI, but the necessity of Newton-Raphson iterations at every grid point greatly limits the application of GPU parallelization.

In the first part of this paper we introduce the evolution equations of a coupled phase field and crystal plasticity model, addressing the solid-solid phase transformation where the eigenstrain of the new phase drives elasto-plastic accommodation in both the matrix and the new phase. In the second part an implementation using two open-source packages are described with the focus on parallelization techniques for the coupling. Finally we present the numerical results of a modified Eshelby's inclusion problem and an application to the $\gamma \rightarrow \alpha$ transformation in iron-based alloys.

2. MODELS

Consider the solid-solid phase transformation during which the mismatch of atomic distances between the product phase and the parent induces a strain field in the vicinity. The minimization of the strain energy is obtained by elasto-plastic deformation in both phases, which affects the transformation kinetics and leads to macroscopic deformation under external loads (transformation induced plasticity effect, or TRIP). In crystalline materials, especially alloys, the plastic accommodation controlled by dislocation slip or mechanical twinning is highly anisotropic and therefore results in lath- or plate-like morphology of the product phases. The phase transformation and the elasto-plastic deformation can be readily captured by the phase-field and crystal-plasticity models, respectively. In this paper a coupled model is proposed to study the mutual interaction of these processes.

2.1. Multi phase-field model

The governing equations of the MPF order parameters $\dot{\phi}_i = f(\{\phi\}, \{\nabla^2\phi\}, \boldsymbol{S})$ developed by Steinbach et al. are used in this model (Steinbach, 2009; Eiken et al., 2006; Tiaden et al., 1998). ϕ_i is the order-parameter field of phase i, which varies from 0 to 1 under the constrain that $\sum_i \phi_i = 1$. The notation $\{\phi\}$ represents the complete set of order parameters $\phi_1, \phi_2, \ldots, \phi_N$. Our focus lies on the coupling between phase field and mechanical models so the heat transfer and solid diffusion equations are not considered. Thus the evolution equation for the order parameters reads

$$\dot{\phi}_i = \sum_j m_{ij} \left\{ \kappa_{ij} \left[\phi_i \nabla^2 \phi_j - \phi_j \nabla^2 \phi_i + \frac{\pi^2}{2\eta^2} (\phi_i - \phi_j) \right] - \frac{\pi}{\eta} \sqrt{\phi_i \phi_j} \Delta g_{ij} \right\} \quad (1)$$

where m, κ and η is the interface mobility, interface tension and interface width, respectively. The free energy difference (driving force) Δg_{ij} of a pair of phases is given by

$$\Delta g_{ij} = G_i - G_j - \frac{1}{2} \boldsymbol{S} : \left(\boldsymbol{F}_{ij}^{*T} \boldsymbol{F}_{ij}^{*} - \boldsymbol{I} \right) \quad (2)$$

The first two terms are the bulk free energies of the two phases and the third is the strain energy density attributed to the transformation-induced strain. The eigenstrain tensor $\boldsymbol{F}_{ij}^{*}$ of the transformation pair is determined by the lattice mismatch and the stress tensor field $\boldsymbol{S}$ comes from the plasticity model.

While the MPF model is readily coupled with thermal conduction and mass diffusion models, in this paper we limit our study to the cases where the phase transformation kinetics is mainly controlled by the elasto-plastic deformation of the matrix so that the pile up of heat and solute ahead of the phase boundary can be neglected.

2.2. Crystal plasticity

The model discussed in this paper follows the CP framework and notations of Roters et al. (2010) and Roters et al. (2011). We starts with the equation of stress balance at every material point under the

quasi-static assumption that the inertia can be neglected,

$$\nabla \cdot \boldsymbol{P} = \boldsymbol{0} \tag{3}$$

where $\boldsymbol{P} = \boldsymbol{FS}$ is the first Piola-Kirchhoff stress. The second Piola-Kirchhoff stress tensor $\boldsymbol{S}$, as a function of deformation gradient tensor and various internal variables $\boldsymbol{S}\left(\boldsymbol{F}, \dot{\boldsymbol{F}}, \{\gamma\}, \{\tau_{\mathrm{CRSS}}\}, \{\phi\}\right)$, is governed by the following kinematic and constitutive equations.

The total deformation gradient tensor $\boldsymbol{F}$ can be decomposed into the elastic, plastic and transformation-induced strain,

$$\boldsymbol{F} = \boldsymbol{F}_e \left(\sum_i \phi_i \boldsymbol{F}_i^* \right) \boldsymbol{F}_p \tag{4}$$

where $\boldsymbol{F}_e$ is the elastic part which determines the stress field through Hooke's law,

$$\boldsymbol{S} = \frac{1}{2} \mathbb{C} : (\boldsymbol{F}_e^T \boldsymbol{F}_e - \boldsymbol{I}) \tag{5}$$

and $\boldsymbol{F}_p$ is the plastic deformation gradient as a tensor sum of the shear of individual slip systems of dislocations,

$$\dot{\boldsymbol{F}}_p \boldsymbol{F}_p^{-1} = \boldsymbol{L}_p = \sum_i \dot{\gamma}_i \boldsymbol{b}_i \otimes \boldsymbol{n}_i \tag{6}$$

The outer product of the normalized Burgers vector $\boldsymbol{b}$ (slip direction) and the slip plane normal $\boldsymbol{n}$ gives the Schmid tensor, which linearly maps the shear rates of slip systems $\dot{\gamma}$ to the overall deformation velocity gradient L_p. On each slip system, the shear is driven by the resolved shear stress $\tau_i = \boldsymbol{S} : (\boldsymbol{b}_i \otimes \vec{\boldsymbol{n}}_i)$, which is the projection of the stress tensor on the slip plane and direction. It can be described by various models (Roters et al., 2011). In the current work, we use the phenomenological power-law equation,

$$\dot{\gamma}_i = \dot{\gamma}_0 \left| \frac{\tau_i}{\tau_i^{\mathrm{CRSS}}} \right|^n \mathrm{sgn}(\tau_i) \tag{7}$$

in which τ^{CRSS} is the critical resolved shear stress (CRSS) with a strain hardening law,

$$\dot{\tau}_i^{\mathrm{CRSS}} = h_0 \left(1 - \frac{\tau_i^{\mathrm{CRSS}}}{\tau_{\mathrm{sat}}} \right)^w \sum_j h_{ij} \dot{\gamma}_j \tag{8}$$

The model parameters n, w, h and τ_{sat} should be calibrated from experimental obtained yield surface and hardening curves.

3. NUMERICAL SOLVERS AND PARALLELIZATION

The stress response $\boldsymbol{P}(\boldsymbol{F})$ of each material point is implicitly given by Eqs. (4-8), which are solved using the Newton-Raphson method with the tensor $\boldsymbol{L}_p$ as optimization parameters. The algorithm is illustrated in figure 1. Since the solution of each grid point is independent of each other, the outer loop can be easily parallelized using OpenMP or MPI. The OpenMP technique was implemented in the open-source package employed in the current study (Roters et al., 2012), the Düsseldorf Advanced Material Simulation Kit (DAMASK). Its latest release starts to support hybrid OpenMP/MPI parallelization. This parallelization strategy applies equally to FEM and spectral method although most FE-targeted implementations rely on the parallelization scheme of the solver. In the following discussion we focus on the spectral method as it is generally considered more computationally efficient. Figure 2 describes a spectral solver using the basic scheme (Diehl, 2010; Eisenlohr et al., 2013; Shanthraj et al., 2015), which involves a forward and a backward FFTs at each iteration. The FFTs are performed on a regular grid with the multi-threaded parallelization provided by the FFTW library (Frigo & Johnson, 2005).

Although the phase-field equations can be solved by various methods (including FE, spectral and FD), the FD method is still the mainstream, especially for multi-phase field applications. In the current work the open-source library, OpenPhase (www.openphase.de), is used, which is parallelized by OpenMP.

We adopt the weak coupling approach by neglecting the term $\partial\phi \,/\, \partial S$ so that the calculation of CP and MPF equations are independent of each other. Therefore, with minor modification to the existing codebase (DAMASK and OpenPhase) both spectral solver and FD solver can run in separated processes or MPI groups of processes. We have developed an inter-processes communication (IPC) library (using system shared memory and MPI) to copy and synchronize the field variables $\boldsymbol{S}$ and ϕ_i between these two solver at the beginning and end of each time step. The overall parallelization of the coupled simulation is similar to the hybrid OpenMP-MPI parallelization.

#pragma omp parallel for ;
forall *grid point* **do**
  Get $\bar{\boldsymbol{F}}_i$, $\boldsymbol{F}_p$ from last time step ;
  repeat
    $\boldsymbol{F}_e = \boldsymbol{F}\boldsymbol{F}_p^{-1}(\boldsymbol{I} - \mathrm{d}t \cdot \boldsymbol{L}_p^{\mathrm{guess}})\bar{\boldsymbol{F}}_i^{-1}$
    $\boldsymbol{S}_{\mathrm{unload}} = \frac{1}{2}\mathbb{C}(\boldsymbol{F}_e^T\boldsymbol{F}_e - \boldsymbol{I})$
    $\boldsymbol{S} = \boldsymbol{F}_i^{-1}(\boldsymbol{S}_{\mathrm{unload}}\boldsymbol{F}_i^{-T})\det(\boldsymbol{F}_i)$
    $\boldsymbol{L}_p, \frac{\partial \boldsymbol{L}_p}{\partial \boldsymbol{S}} = \mathrm{PhenomenologicalLaw}(\boldsymbol{S})$
    $\mathrm{error}(\boldsymbol{L}_p) = \boldsymbol{L}_p^{\mathrm{guess}} - \boldsymbol{L}_p$
    Correct $\boldsymbol{L}_p^{\mathrm{guess}}$ by $\frac{\partial \boldsymbol{L}_p}{\partial \boldsymbol{S}}$
  until $\mathrm{error}(\boldsymbol{L}_p) < \mathrm{tolerance}$;
end

Algorithm 1: *Newton-Raphson loop for solving stress response at each grid point*

The choice of time step which ensures stable solution is determined by the stiffness of the equations and the numerical methods. For the coupled model at hand, the critical time step for the MPF model is 1 to 2 order of magnitude smaller than the CP model but its computational cost is also significantly lighter. An efficient implementation should use different time discretization separately for FD and spectral method. A synchronization barrier is inserted where one software tries to access the variables of the other. The process will be put into sleeping state by the operating system when its step time (at the end of the current step) is ahead of the counterpart. Linear interpolation and extrapolation are employed to calculate the variables at mismatched time steps. Figure 1 shows an overview of the parallelization scheme.

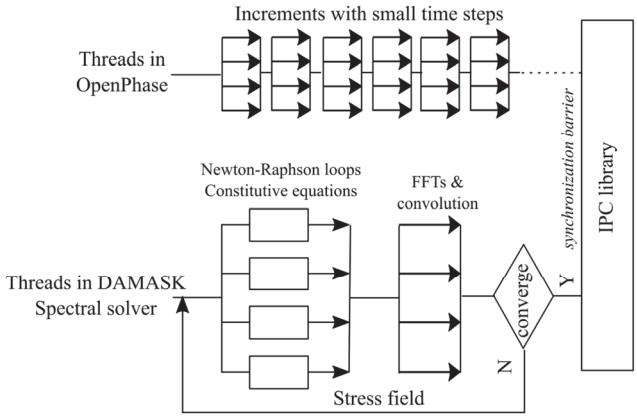

Fig. 1. *Overview of the hybrid parallelization methods for coupled CP&PF model. The lower part represents a single time increment of the spectral solver*

4. NUMERICAL EXAMPLES

4.1. Spherical inclusion with volumetric expansion

In the first example we simulate the stress and strain fields caused by a spherical inclusion with isotropic volumetric expansion of 15.7% (eigenstrain $\boldsymbol{F}^* = 1.05\boldsymbol{I}$). For simplicity, both the matrix and the inclusion have a face-centered cubic (FCC) structure with the [100] crystallographic direction parallel to the x, y and z axis of the system. Thus the system preserves all the rotational symmetries of the cubic crystal system. While the growing or shrinkage of the inclusion are not considered in this example, mechanical loading is accomplished by increasing the order parameter gradually from

Data: input $\boldsymbol{F}_{\mathrm{BC}}$ and $\boldsymbol{P}_{\mathrm{BC}}$
Result: $\boldsymbol{F}(\boldsymbol{x})$ and $\boldsymbol{P}(\boldsymbol{x})$ such that $\bar{\boldsymbol{F}}(\boldsymbol{x}) = \boldsymbol{F}_{\mathrm{BC}}$ and $\bar{\boldsymbol{P}}(\boldsymbol{x}) = \boldsymbol{P}_{\mathrm{BC}}$
while $\mathrm{error}_{\mathrm{divergence}} > \mathrm{tol}$ ***or*** $\mathrm{error}_{\mathrm{stress}} > \mathrm{tol}$ **do**
  $\boldsymbol{P}(\boldsymbol{x}) = f(\boldsymbol{F}(\boldsymbol{x}))$; // constitutive law
  $\hat{\boldsymbol{P}}(\boldsymbol{k}) = \mathscr{F}[\boldsymbol{P}(\boldsymbol{x})]$; // Fourier transformation
  $\boldsymbol{F}(\boldsymbol{x}) \mathrel{-}= \mathscr{F}^{-1}\left(\begin{cases} \boldsymbol{\Gamma}(\boldsymbol{k})\hat{\boldsymbol{P}}(\boldsymbol{k}) & \text{if } k \neq 0 \\ \Delta\boldsymbol{F}_{\mathrm{BC}} & \text{if } k = 0 \end{cases}\right)$;
  // apply the Green operator $\boldsymbol{\Gamma}(\boldsymbol{k})$
end

Algorithm 2: *A spectral method using the basic scheme (Eisenlohr et al., 2013; Diehl,2010; A. Lebensohn, 2001; Shanthraj et al., 2015)*

zero to one. We use the sample material parameters which are provided by Eisenlohr et al. (2013) and shown in table 1. Periodic boundary conditions are applied to all directions with $\overline{\boldsymbol{F}} = \boldsymbol{I}$, which is equivalent to fixed boundary conditions due to the cubic symmetry of the system.

Table 1. *Model parameters for the example of spherical inclusion (Eisenlohr et al., 2013)*

Symbol	Description	Value
$\varphi_1, \Phi, \varphi_2$	Euler angles for both phases	*0, 0, 0*
$N_x \cdot N_y \cdot N_z$	Grid size	64 × 64 × 64
N_{slip}	Number of slip system	12 (FCC)
$\dot{\gamma}_0$	Referential glide velocity	0.001
$\tau^{\text{CRSS}}(t = 0)$	Initial CRSS	31 MPa
τ_{sat}	Saturation CRSS	63 MPa
h_0	Hardening parameter	75 MPa
h_{ij}	Cross hardening (same slip plane)	1
h_{ij}	Cross hardening (other slip plane)	1.4
n	Exponent resolved shear stress	20
w	Exponent hardening	2.25
$\mathbb{C}_{11}$	Elastic constant	106.75 GPa
$\mathbb{C}_{12}$	Elastic constant	60.41 GPa
$\mathbb{C}_{44}$	Elastic constant	28.34 GPa
η	Interface Width	5 grid points
r_0	Inclusion radius	10

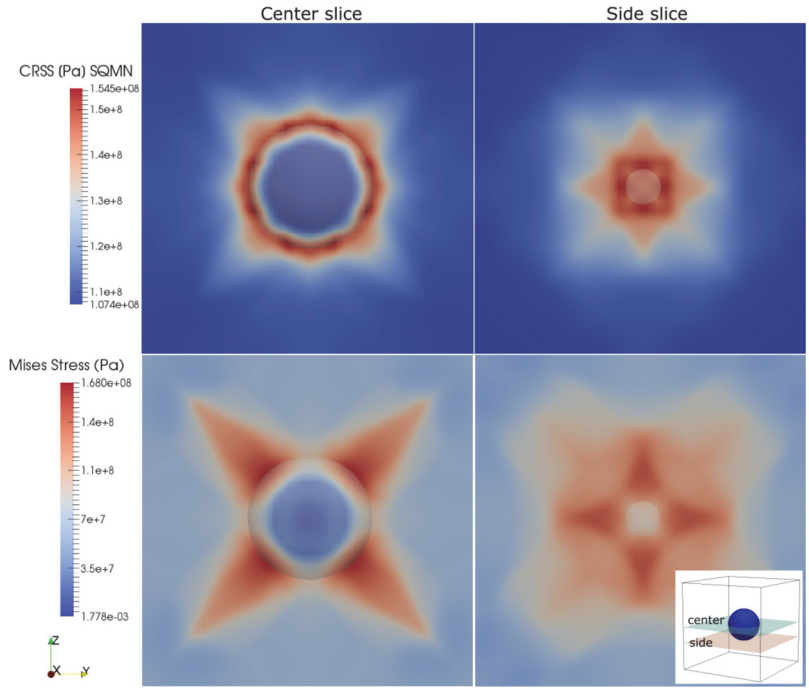

Fig. 2. *Stress distribution at two slices across the inclusion. Top: root sum square of the critical resolved shear stresses of all slip systems; Bottom: von Mises stress. The position of slices is shown at the bottom right.*

The stress response of the matrix is shown in figure 2. The stress and the root sum square of the CRSS of all slip systems are plotted on two slices of the 3D domain. Due to symmetry they represent 9 equivalent slices of the domain. As expected, we observe highly anisotropic behavior compared to the classical Eshelby's solution. Long tails of high stress region stretch out from the inclusion center along all the 6 slip directions. Similar patterns appear in the CRSS map which reflects the distribution of local strain hardening. The highlighted regions in the CRSS map are active slip bands that experienced higher degree of plastic deformation. Their influences on the phase transformation kinetics and morphologies are demonstrated in the following example.

4.2. Austenite to ferrite transformation in iron based alloy

As an example with more practical interest, we investigate the displacive transformations (e.g. bainitic and martensitic transformations) from austenite γ to ferrite α in iron based alloys. Austenite and ferrite have different crystal structures (respectively FCC and BCC). Hence there is a misfit of slip planes and directions. The selection of certain crystallographic planes for plastic accommodation gives rise to the special morphology of ferrite. In this session we use the aforementioned model to investigate the effect of slip selection on a growing ferrite grain. Since nucleation process cannot be readily captured by phase field model, a spherical nuclei of ferrite is placed in the austenite grain. The initial stress balance is established by the same approach as in the above example of spherical inclusion. The initial orientation and eigenstrain of the ferrite are set to experimental observed values (Kundu et al., 2007). Following the simple model of Bain strain (Bhadeshia, H. K. D. H, 2001), the deformation of ferrite can be roughly described by contraction strain in one of the $[100]_\gamma$ crystallographic directions and expansion strain in the other two. This contraction direction is aligned parallel to the z-axis in this simulation. With the free energy functions provided by the TEFE steel database of Thermo-Calc and the crystal plasticity parameters determined from room- and high temperature tensile curves, the material parameters for this example are listed in table 2.

Table 2. *Model parameters for the austenite to ferrite transformation*

Symbol	Description	Value for ferrite	Value for austenite
$\varphi_1, \Phi, \varphi_2$	Euler angles (degree)	*0.366, 8.318, 6.756*	*-45, 0, 0*
$\dot{\gamma}_0$	Referential glide velocity	0.001	0.001
τ^{CRSS}	Initial CRSS	55 MPa	60 MPa
τ_{sat}	Saturation CRSS	205 MPa	210 MPa
h_0	Hardening parameter	312 MPa	150 MPa
h_{ij}	Cross hardening (same slip plane)	1	1
h_{ij}	Cross hardening (other slip plane)	1.4	1.4
n	Exponent resolved shear stress	20	20
w	Exponent hardening	1.0	2.25
$\mathbb{C}_{11}$	Elastic constant	223.3 GPa	185.0 GPa
$\mathbb{C}_{12}$	Elastic constant	135.5 GPa	104.4 GPa
$\mathbb{C}_{44}$	Elastic constant	118.0 GPa	49.0 GPa
G_i	Bulk free energy	- 56.4 J/cm3	0
F^*	Eigenstrain tensor	$\begin{pmatrix} 1.1173 & -0.0331 & 00973 \\ 0.0176 & 1.1189 & 0.0893 \\ -0.1404 & -0.1232 & 0.7853 \end{pmatrix}$	

Figure 3 shows the stress field induced by the growing ferrite and the phase boundary traces at different time steps. It can be observed that 3 pairs of phase boundary facets are developed as a consequence of the interaction between stress field and the phase evolution. These facets are determined by the slip systems of both the FCC and BCC crystals. The code performance with 1 to 14 threads is shown in figure 1 where the runtime of the simulation reduces effectively with up to 10 threads. Although additional threads provide insignificant benefit in this example, they would improve the performance of the simulation with a larger problem size.

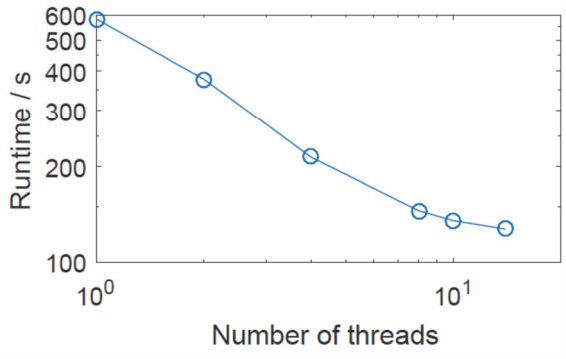

Fig. 4. *Code performance test with up to 14 threads: Computation time for 23 iterations in example 2 (Intel compiler 15, Intel Xeon E5-2695-v3)*

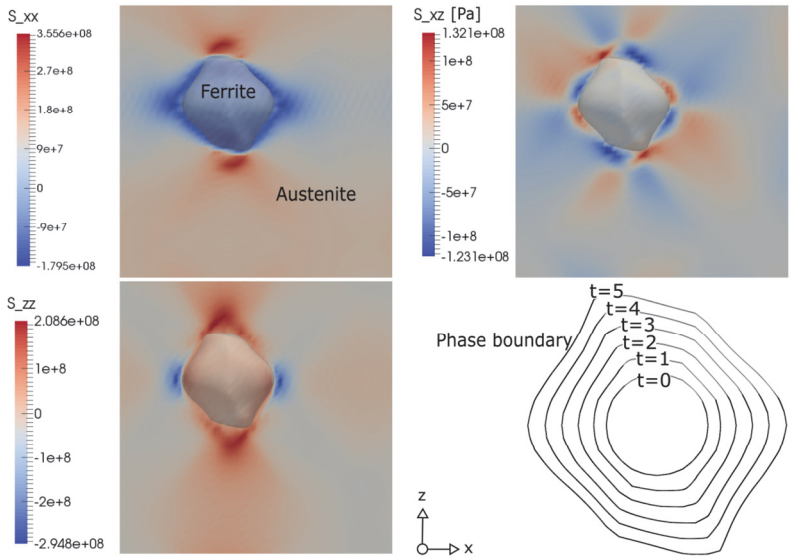

Fig. 3. *Stress field around a growing ferrite. The 3D stress field is sliced along the x-z plane through the center of the ferrite grain. The bottom right figure shows the traces of the phase boundary at different time steps.*

5. SUMMARY

A mutually interacted phase-field and crystal plasticity model has been demonstrated with an implementation using finite difference and spectral methods in parallel. The given numerical examples regarding solid-solid phase transformation show that the model is able to capture the anisotropic mechanical response and transformation morphology determined by the slip systems of the crystal. We have introduced a hybrid-parallelization technique, where the underlying software packages, OpenPhase and DAMASK, run in separated process spaces with extensive OpenMP parallelization and communicate via the system shared memory. The inter-processes communication library allows heterogeneous

time stepping for optimized balance between computational performance and numerical stability. A code performance test with a 64^3 grid shows effective run-time reduction with up to 10 threads.

ACKNOWLEDGMENTS

This work has been supported by the Deutsche Forschungsgemeinschaft (DFG) under the priority program SPP 1713, with project M7 - "Modelling bainitic transformations during press hardening". The authors gratefully acknowledge the computing time granted by the JARA-HPC Vergabegremium and provided on the JARA-HPC Partition part of the supercomputer at RWTH Aachen University.

REFERENCES

Arif, T. T. Qin, R. S., 2013, A phase-field model for bainitic transformation, *Computational Materials Science*, 77, 230-235.

Arif, T. T. Qin, R. S., 2014, A Phase-Field Model for the Formation of Martensite and Bainite, *Advanced Materials Research*, 922, 31-36.

Bhadeshia, H. K. D. H, 2001, *Worked examples in the geometry of crystals*, Institute of Metals, Brookfield and VT and USA, 2nd edition.

Cahn, J. W. Hilliard, J. E., 1958, Free Energy of a Nonuniform System. I. Interfacial Free Energy, *The Journal of Chemical Physics*, 28(2), 258.

Diehl, M., 2010, *A spectral method using fast Fourier transform to solve elastoviscoplastic mechanical boundary value problems*, Master's thesis, Technische Universitaet Muenchen, Munich.

Eiken, J., Böttger, B., Steinbach, I., 2006, Multiphase-field approach for multicomponent alloys with extrapolation scheme for numerical application, *Physical Review E*, 73(6).

Eisenlohr, P., Diehl, M., Lebensohn, R. A., Roters, F., 2013, A spectral method solution to crystal elasto-viscoplasticity at finite strains, *International Journal of Plasticity*, 46, 37-53.

Frigo, M. Johnson, S. G., 2005, The Design and Implementation of FFTW3, *Proceedings of the IEEE*, 93(2), 216-231.

Kundin, J., Pogorelov, E., Emmerich, H., 2015, Numerical investigation of the interaction between the martensitic transformation front and the plastic strain in austenite, *Journal of the Mechanics and Physics of Solids*, 76, 65-83.

Kundin, J., Raabe, D., Emmerich, H., 2011, A phase-field model for incoherent martensitic transformations including plastic accommodation processes in the austenite, *Journal of the Mechanics and Physics of Solids*, 59(10), 2082-2102.

Kundu, S., Hase, K., Bhadeshia, H., 2007, Crystallographic texture of stress-affected bainite, *Proceedings of the Royal Society A, Mathematical, Physical and Engineering Sciences*, 463(2085), 2309-2328.

Ma, A., Roters, F., Raabe, D., 2006, On the consideration of interactions between dislocations and grain boundaries in crystal plasticity finite element modeling – Theory, experiments, and simulations, *Acta Materialia*, 54(8), 2181-2194.

Prakash, A. Lebensohn, R. A., 2009, Simulation of micromechanical behavior of polycrystals, finite elements versus fast Fourier transforms, *Modelling and Simulation in Materials Science and Engineering*, 17(6), 064010.

Qin, R. S. Bhadeshia, H., 2009, Phase-field model study of the effect of interface anisotropy on the crystal morphological evolution of cubic metals, *Acta Materialia*, 57(7), 2210-2216.

Roters, F., Eisenlohr, P., Bieler, T. R., Raabe, D., 2011, *Crystal Plasticity Finite Element Methods, In Materials Science and Engineering*, Wiley, Somerset.

Roters, F., Eisenlohr, P., Hantcherli, L., Tjahjanto, D. D., Bieler, T. R., Raabe, D., 2010, Overview of constitutive laws, kinematics, homogenization and multiscale methods in crystal plasticity finite-element modeling, Theory, experiments, applications, *Acta Materialia*, 58(4), 1152-1211.

Roters, F., Eisenlohr, P., Kords, C., Tjahjanto, D. D., Diehl, M., Raabe, D., 2012, DAMASK, the Düsseldorf Advanced MAterial Simulation Kit for studying crystal plasticity using an FE based or a spectral numerical solver, *Procedia IUTAM*, 3, 3-10.

Shanthraj, P., Eisenlohr, P., Diehl, M., Roters, F., 2015, Numerically robust spectral methods for crystal plasticity simulations of heterogeneous materials, *International Journal of Plasticity*, 66, 31-45.

Steinbach, I., 2009, Phase-field models in materials science, *Modelling and Simulation in Materials Science and Engineering*, 17(7), 073001.

Steinbach, I. Apel, M., 2006, Multi phase field model for solid state transformation with elastic strain, *Physica D, Nonlinear Phenomena*, 217(2), 153-160.

Steinbach, I. Pezzolla, F., 1999, A generalized field method for multiphase transformations using interface fields, *Physica D, Nonlinear Phenomena*, 134(4), 385-393.

Tiaden, J., Nestler, B., Diepers, H. J., Steinbach, I., 1998, The multiphase-field model with an integrated concept for modelling solute diffusion, *Physica D, Nonlinear Phenomena*, 115(1-2), 73-86.

RÓWNOLEGŁY MODEL DLA SYMULACJI METODAMI SPRZĘŻONEGO POLA FAZ I PLASTYCZNOŚCI KRYSZTAŁÓW

Streszczenie

Uzyskanie realistycznych możliwości obliczeniowych modeli materiałowych łączących rozwój mikrostruktury z odkształceniami wymaga sprzężenia dwóch lub więcej modeli fizycznych. Sprzężenie między modelem pola faz i różnymi modelami mechanicznymi jest ostatnio w obszarze zainteresowania naukowców. W pracy zaproponowano sprzężenie modelu pola wielofazowego z modelem plastyczności kryształów, który uwzględnia anizotropię zachowania się materiałów polikrystalicznych. Różnica w złożoności obliczeniowej i w wymaganiach dla solwera pomiędzy tymi modelami jest wyzwaniem dla sprzężenia i zrównoleglenie obliczeń. Zaproponowana w pracy metoda umożliwia zrównolegleni obliczeń z wykorzystaniem dwóch modeli poprzez zastosowanie solwerów numerycznych z różną dyskretyzacją czasu. Dwa przykłady będące zastosowaniem dla przemiany austenit-ferryt w stopach żelaza są podsumowaniem pracy.

Received: August 31, 2016
Received in a revised form: November 15, 2016
Accepted: November 30, 2016